Design and Implementation of a Bipolar-Unipolar Switched Boundary Current Mode (BCM) Control GaN-Based Single-Phase Inverter

Kamal Sabi, Daniel Costinett
Min H. Kao Department of Electrical Engineering and Computer Science
The University of Tennessee
Knoxville, TN USA
ksabi@vols.utk.edu

***Abstract*—This paper presents the design and implementation of a boundary current mode (BCM) modulated GaN-based single phase inverter using a combination of bipolar and unipolar switching. Both unipolar and bipolar BCM-switched full bridge inverters are explored in detail in the context of efficiency, output current distortion and leakage current. Although the unipolar switched BCM inverter results in a higher efficiency in comparison to the bipolar switched inverter, it leads to a higher output current distortion at the low frequency zero crossing. On the other hand, the bipolar switched BCM inverter yields a low leakage current and reduced output current distortion, but exhibits lower efficiency. To overcome the low frequency zero crossing current distortion while maintaining a high efficiency, a combination of bipolar and unipolar switching in a BCM inverter is proposed. An experimental prototype has been built to validate the proposed control technique and modulation scheme. The proposed approach achieves a 2% efficiency improvement in comparison to the standard bipolar switched BCM inverter and a THD of 1.15%.**

***Index Terms*—Single-phase inverter, boudary current mode (BCM), zero voltage switching (ZVS), gallium nitride (GaN).**

I. Introduction

High power density and high efficiency converters are two important design target in power electronics for many modern applications such as electric vehicles and renewable energy. Recent trend have put an emphasis on reducing the size of inverters and rectifiers for residential and commercial grid tied application. A smaller and lighter inverter can reduce the size of the overall system and the associated cost of installation and maintenance [1–3]. To achieve this goal, a common single-phase full bridge inverter operating at high switching frequency is often used. However, the high switching frequency results in high power loss and more severe electromagnetic interference (EMI) limiting the maximum switching frequency in practice [2, 4]. To overcome these challenge, soft switching techniques such as boundary current mode (BCM) control is used in inverters to realize zero voltage switching (ZVS) operation and minimize switching losses [5–8].

The basic operation principle of the BCM inverter is illustrated in [8, 9]. To achieve ZVS operation with minimal current stresses, the inductor current is controlled in a full bridge topology to follow the envelop wave shape shown in Fig. 1. BCM modulation exhibits cycle-by-cycle inductor current polarity inversion, facilitating operation with zero-voltage switching of all semiconductor devices. This feature can be used to increase switching frequency in order to reduce the size of passive components, to increase efficiency by greatly reducing switching losses, or a combination of the two [5, 6, 10–13].

BCM modulation can be achieved using either unipolar or bipolar switching schemes. Regardless of switching operation, efficiency and output current distortion are two important factors governing the design of the inverter [14]. In addition, other challenges associated with the switching strategy include the presence of common mode (CM) noise and leakage current, which can cause safety issue, increase system loss, and induce electromagnetic interference (EMI) [15–17].

Both unipolar and bipolar switched BCM inverters for off-grid applications have been explored in detail in the context of low frequency output current distortion, efficiency, leakage current and common mode voltage. The unipolar switched inverter has the advantage of low switching loss; however, it has a significant distortion of the output current at the zero crossing as well as significant CM noise [14, 18]. Although the bipolar switched inverter has almost non-existent high frequency CM noise and zero-crossing output current distortion, it has the disadvantage of low efficiency due to increased switching loss [14]. Taking advantage of the benefits of both switching schemes, while also mitigating their respective challenges, a combination of bipolar and unipolar switching is investigated for a BCM single phase inverter. The proposed technique eliminates the low frequency output current at the zero crossing while improving efficiency by 2% in comparison to a standard bipolar switched BCM inverter. The remainder of this work is organized as follows. First, both unipolar and bipolar BCM modulation switching techniques are discussed in Section II, followed with the proposed switching approach in Section III. Second, the loss model of the proposed switching technique is discussed in Section IV. Then, the experimental results are presented in Section V. Finally, the conclusions and future works are stated in Section VI.

978-1-7281-0395-2/19/$31.00

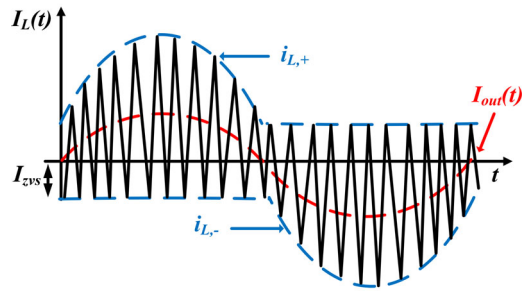

Fig. 1. BCM modulation inductor current waveform with fixed reverse ZVS current I_{zvs}.

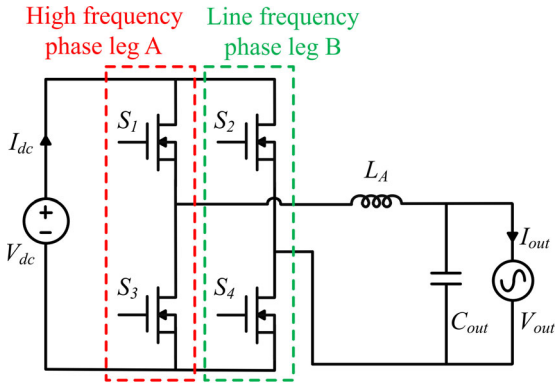

Fig. 2. Full bridge inverter topology for unipolar switched BCM inverter.

II. BCM Control Switching Method

Unipolar and bipolar switching are the two common switching technique used in a BCM inverter. The operation principle of both switching approaches including their respective advantages and disadvantages is demonstrated. For the following analysis, the average value of the dc-link voltage V_{dc} is assumed to be 250V, the RMS output voltage V_{out} is 120V, and the line frequency is 60 Hz. In addition, the analysis assumes a fixed reverse ZVS current I_{zvs}.

A. BCM with Unipolar Switching

The typical full bridge topology used in a unipolar switched BCM control inverter is shown in Fig. 2. This topology uses an asymmetrical inductor configuration, consisting of one inductor on the high switching phase leg A. The phase leg A devices, S_1 and S_3, operate at high switching frequency while the phase leg B switches, S_2 and S_4, operate at line frequency. During the positive half line cycle, S_4 is on and S_2 is off and vice-versa during the negative half cycle. During the output current zero crossing, all switches are turned off. For a given positive and negative peak inductor current $I_{L,+}$ and $I_{L,-}$, the ON/OFF time with reference to the active switch are

$$t_{on} = \frac{L \cdot (I_{L,+} - I_{L,-})}{V_{dc} - V_{out}} \tag{1}$$

$$t_{off} = \frac{L \cdot (I_{L,+} - I_{L,-})}{V_{out}} \tag{2}$$

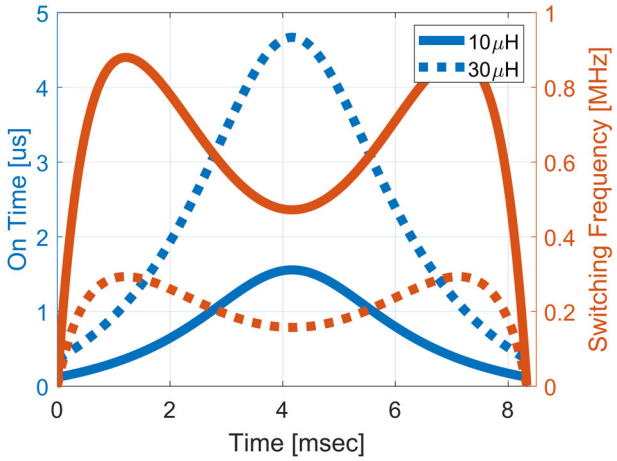

Fig. 3. On time t_{on} and switching frequency f_s for 10 µH and 30 µH inductor in a unipolar switched BCM inverter during the positive half line cycle.

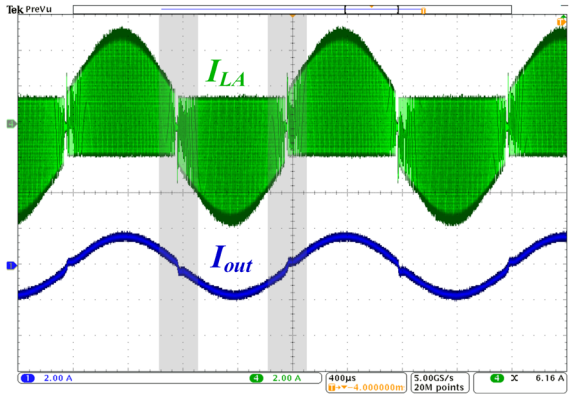

Fig. 4. Experimental inductor current I_{LA} and output current I_{out} waveform of unipolar switched BCM inverter showing output current distortion at the zero crossing.

which result in a switching frequency which varies over the line cycle,

$$f_s = \frac{V_{out} \cdot (V_{dc} - V_{out})}{V_{dc} \cdot L \cdot (I_{L,+} - I_{L,-})} \tag{3}$$

For a fixed ZVS current I_{zvs}, Fig. 3 shows how the ON time, t_{on} and switching frequency f_s vary for two inductances, 10 µH and 30 µH during the positive half-cycle. For instance, for an inductance L_A of 10 µH, the minimum ON time and switching frequency converge to zero at the zero crossing. When the switching frequency is at its peak value of 880 kHz, t_{on} is approximately 370 ns. Unipolar switching can only demagnetize the inductor current at a rate of V_{out}/L. In a standalone system when the output voltage V_{out} approaches zero, the switching frequency converges to zero causing a distortion of the current and a potential loss of regulation [19]. This undesirable issue requires the implementation of additional control to ensure BCM waveforms and output regulation are maintained or minimally distorted during the

output voltage zero crossing. Fig. 4 illustrates an experimental waveform of the output current distortion at the zero crossing.

This switching scheme yields a pulsating CM voltage at the output of the inverter, thus contributing to CM noise and leakage currents [20]. Topologies such as the H5, H6, and HERIC alleviate issues with leakage currents in unipolar switched transformerless inverters through the use of additional switches; however, the bipolar switched BCM full bridge does not exhibit the same leakage current issues when using balanced output impedances [20].

B. BCM with Bipolar Switching

To overcome the zero crossing regulation and leakage current issues present with unipolar switched BCM inverter, a bipolar switching technique is often used. The topology for the bipolar switched BCM full bridge inverter is shown in Fig. 5 with a symmetrical inductor configuration. The inductance is split between both phase legs to balance impedances and mimimize common-mode effects. The total equivalent inductance is $L_{eq} = L_A + L_B$. In contrast to unipolar switched BCM inverter, both phase leg A and B are switched at high frequency. Switches S_1 and S_4 are switched in unison at high switching frequency, and complimentary to S_2 and S_3. The turn ON/OFF time of the active switches are

$$t_{on} = \frac{L \cdot (I_{L,+} - I_{L,-})}{V_{dc} - V_{out}} \tag{4}$$

$$t_{off} = \frac{L \cdot (I_{L,+} - I_{L,-})}{V_{dc} + V_{out}} \tag{5}$$

and the switching frequency is

$$f_s = \frac{V_{dc}^2 - V_{out}^2}{2V_{dc} \cdot L \cdot (I_{L,+} - I_{L,-})} \tag{6}$$

As Illustrated in Fig. 6, the frequency does not drop to zero at the output current zero crossing. Because the zero-state is not employed in bipolar modulation (i.e. the differential output is always $\pm V_{dc}$), inductor demagnitization occurs in finite time as long as $|V_{out}| < V_{dc}$. Therefore, the current distortion observed in the unipolar switching case does not occur in the bipolar case. For an inductance L_A and L_B of 10 µH as in the unipolar switching case, the resulting equivalent inductance L_{eq} is 20 µH. Despite doubling the equivalent inductance in this case, the minimum ON time is around 240 ns while the maximum switching frequency is approximately 2.1 MHz. The resulting maximum switching frequency in this case more than double that of the unipolar, resulting in increased switching loss when both modulations achieve ZVS. The common mode voltage in this switching scheme has no high frequency variation; thus, the CM noise and leakage current is nearly eliminated [17, 20].

Although the bipolar switched BCM inverter helps mitigate current distortion at the zero crossing and minimize leakage current, it results in lower efficiency due to the high switching loss [14]. A combination of both unipolar and bipolar switched BCM inverter is proposed to help improve efficiency, eliminate current distortion and minimize leakage current.

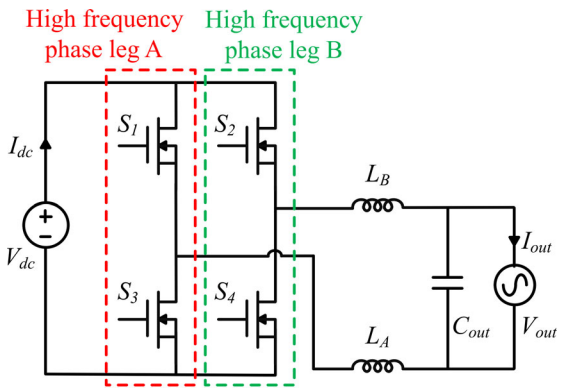

Fig. 5. Full bridge inverter topology for bipolar switched BCM inverter.

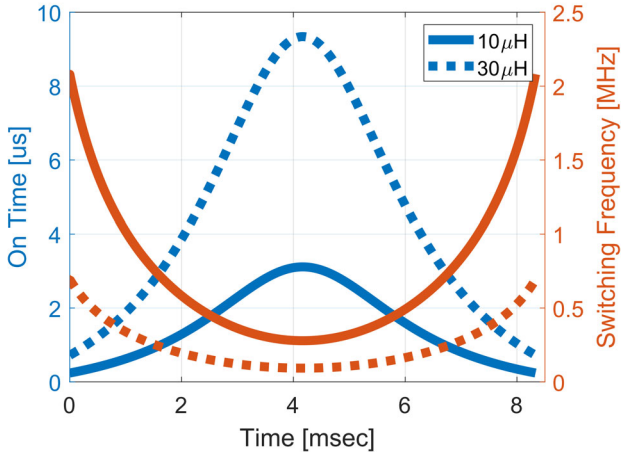

Fig. 6. On time t_{on} and switching frequency f_s for 10 µH ($L_{eq} = 20\ \mu H$) and 30 µH ($L_{eq} = 60\ \mu H$) inductor in a bipolar switched BCM inverter during the positive half line cycle.

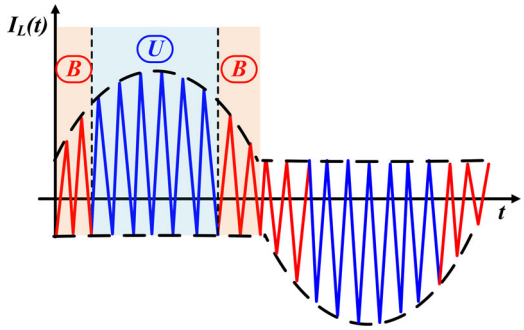

Fig. 7. Proposed bipolar-unipolar switched BCM modulation waveform with fixed reverse ZVS current I_{zvs}.

III. Bipolar-Unipolar Switched BCM Control Inverter

A. Basic Operation

Fig. 7 shows the proposed BCM inductor waveform using a combination of bipolar and unipolar switching technique. The modulation technique consists of using unipolar switch-

ing (U) during the high current sections of the line cycle and bipolar switching (B) at the zero crossing. Using bipolar modulation near the zero-crossing eliminates issues related to zero-crossing distortion inherent to unipolar modulation, while unipolar switching at high currents reduces switching losses. The transition between unipolar and bipoloar modulation occurs when the unipolar switching ON time falls below a specified minimum $t_{on,min}$.

Because BCM modulation achieves ZVS for all switching actions, remaining switching loss mechanisms are dominated by turn-off loss and deadtime reverse conduction, both of which increase significantly at high currents and are proportional to switching frequency. Thus, confining bipolar operation to the low-current portion of the line cycle will minimize the resulting impact on switching losses.

As previously noted, in the unipolar switched topology, there is only one high switching frequency phase leg with an asymmetrical inductor configuration. On the other hand, during bipolar switching, both phase legs are operated at high switching frequency with equal inductance on both phase A and B. Given two sets of inductor configuration in a full bridge topology depending on the switching method, the implementation of the bipolar-unipolar switching technique on either the single-inductor topology in Fig. 2 or the split-inductor topology of Fig. 5 will result in oscillations in the opposite mode.

B. Hardware Implementation

When the bipolar-unipolar switching technique is implemented using the full bridge topology with the asymmetrical inductor configuration illustrated in Fig. 2, it introduces a high frequency common mode voltage during the bipolar switching mode [17]. Phase leg B, previously switched at line frequency during unipolar operation, is now switching at high frequency during bipolar operation near the zero crossing. This operation, with only a single inductor, allows the high frequency voltage at the switch node V_B to directly connect to one terminal of the output, resulting in significant common mode variation and excitation of any parasitic grounding capacitance at the switching frequency. This issue is mitigated by using a symmetrical inductor configuration with an inductor on each phase leg as in bipolar switched BCM full bridge topology in Fig. 5.

Although the symmetrical inductor configuration addresses the high frequency common mode issue, it now introduces a resonance between the phase B inductor L_B and the parasitic grounding capacitance of the output during unipolar switching operation.

To overcome these challenge, an additional phase leg C is introduced as illustrated in Fig. 8. Phase A and B are operated at high switching frequency during bipolar switching while phase C is operated at line frequency during unipolar switching. This hardware solution mitigates the high frequency CM voltage issue during bipolar switching and the resonance problem during unipolar switching. However, the additional phase leg increases the component count and changes the equivalent inductance during each switching mode. During

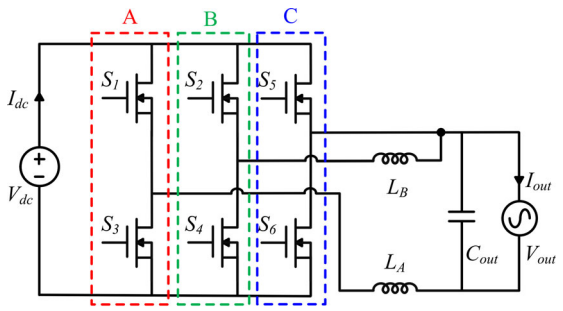

Fig. 8. Full bridge inverter topology for proposed bipolar-unipolar switched BCM inverter.

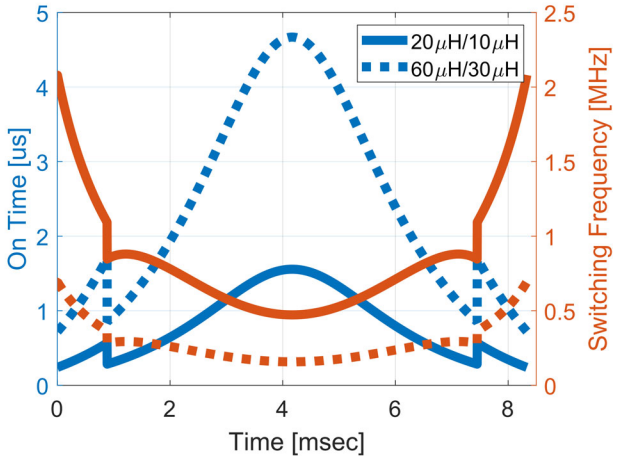

Fig. 9. On time t_{on} and switching frequency f_s for an equivalent inductance of 20 μH/10 μH and 60 μH/30 μH in a bipolar-unipolar switched BCM inverter during the positive half line cycle.

bipolar switching, the equivalent inductance $L_{eq} = L_A + L_B$; during unipolar switching the equivalent inductance is half as large, $L_{eq} = L_A$. The resulting switching frequency and ON time for two sets of inductances are shown in Fig. 9. The frequency is at its maximum at the zero crossing when using bipolar switching and does not converge to zero. Everywhere else, the frequency distribution is given by the unipolar switching.

C. Tradeoff Between Standard Bipolar and Bipolar-Unipolar Switching Technique

When compared with standard bipolar switched BCM inverter, first, the switching frequency during the unipolar switching phase in the proposed approach is slightly higher. As illustrated in Fig. 10, for an equivalent inductance L_{eq} of 20 μH the switching frequency of the proposed switching scheme is larger during the unipolar phase. The increased switching frequency during the unipolar switching phase is due to the half reduction of the inductance. This slight increase in frequency has a minimal effect on the device switching loss because during the unipolar operation, only two devices are switched at high frequency rather than the four in bipolar, resulting in reduced switching losses.

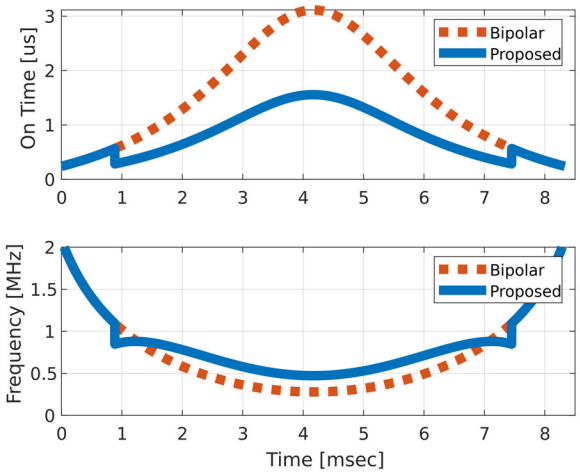

Fig. 10. On time t_{on} and switching frequency f_s for an equivalent inductance of 20 µH in a standard bipolar and 20 µH/10 µH in a proposed bipolar-unipolar switched BCM inverter during the positive half line cycle.

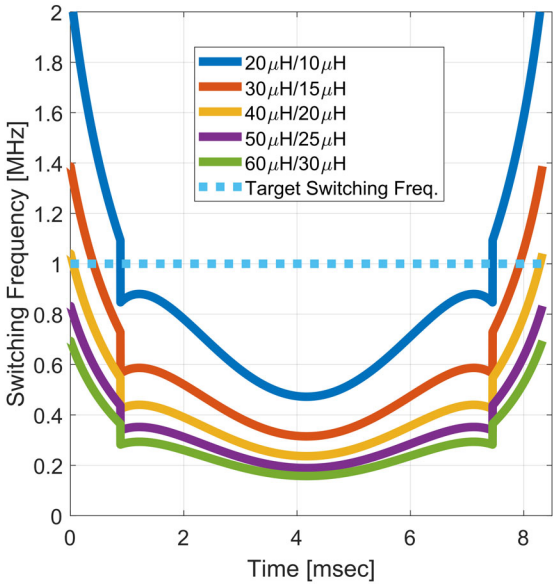

Fig. 11. Switching frequency f_s for a varied set of inductances $2L_A/L_A$ in a proposed bipolar-unipolar switched BCM inverter during the positive half line cycle.

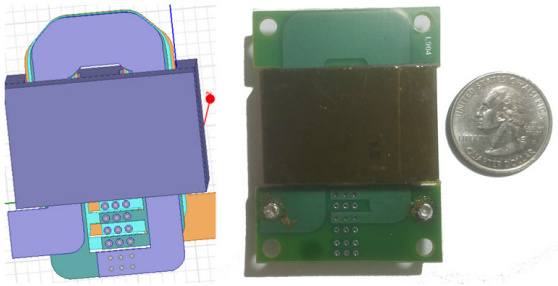

Fig. 12. Q3D model and designed 20 µH planar inductor using EI38 planar core and 3F4 ferrite material.

Second, the hardware implementation of the proposed switching technique introduces additional control complexity and requires careful consideration of current commutation during the transition between the switching phases. If not timed correctly, this may introduce some distortion of the output current, causing an increase in THD. In comparison to bipolar switched BCM inverter, the proposed bipolar-unipolar switching technique is a tradeoff between efficiency and THD.

IV. CONVERTER LOSS MODEL

To analyze the impact of the switching scheme on the converter efficiency, the devices and inductor losses are estimated and the efficiency between the standard bipolar switched BCM inverter is compared with the bipolar-unipolar switching model.

A. Switching Frequency

In this design, the switching frequency range is limited by the minimum ON time during the bipolar switching phase at light loads. For noise immunity and a good control performance, a minimum ON/OFF time of 200 ns and a maximum switching frequency of 1 MHz are selected. These limits constrain the selection of inductance value. Fig. 11 shows the frequency distribution during the positive half-cycle for different inductance combinations during bipolar/unipolar switching. The 40 µH/20 µH inductance combination is within design specification and has been selected. Although larger inductance values above the 40 µH/20 µH combination also satisfy the design constraint, they have not been considered because they require either more volume or exhibit more core loss.

B. Converter Switching and Magnetic Loss

An analytical loss model of the inverter, including the inductor, device and shunt resistor is developed. Based on the applied switching technique, both the inductor core loss and device switching and conduction loss are the main contributor to the power loss. Other forms of loss do not vary significantly with different switching techniques. After surveying available planar cores for high frequency, high power applications, an EI38 planar core made from 3F4 ferrite material from Ferroxcube is used to implement the two 20 µH inductors. Based on the planar inductor design outlined in [21, 22] and the loss model, a 4-turn, 2 oz profiled copper trace winding is used to achieve a 20 µH inductance. The inductor Q3D model and implementation is shown in Fig. 12.

The AC resistance of the winding is estimated using a finite element analysis tool and measured experimentally with an impedance analyzer. The core loss P_{fe} is estimated using the Steinmetz Equation for every switching period and averaged over the line cycle as shown in the following equation:

$$P_{fe} = \frac{2A_c \cdot l_m}{\pi} \int_0^{\pi} (K \cdot f_s(\theta)^{\alpha} \cdot \Delta B(\theta)^{\beta}) d\theta \qquad (7)$$

A_c represent the core cross sectional area and l_m is the

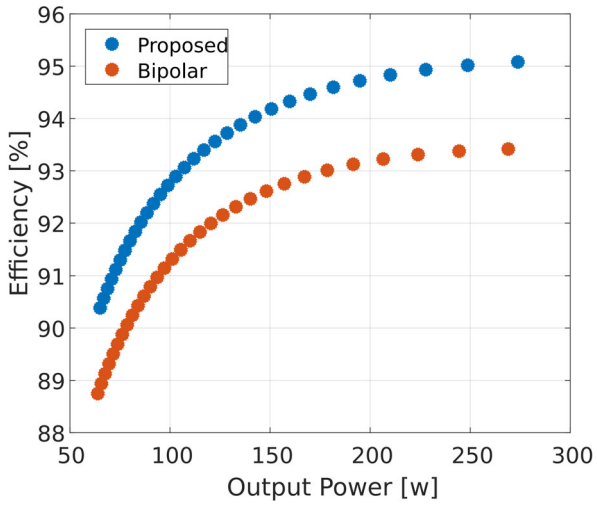

Fig. 13. Analytical efficiency comparision between the standard bipolar switched and proposed bipolar-unipolar switched BCM inverter.

TABLE I
PARAMETERS OF PROTOTYPE

Parameter	Value
Input voltage V_{dc}	250V
Output voltage V_{out}	120V/60Hz
Device	Panasonic GaN-GIT
Inductor L_A, L_B	20μH
Shunt Resistor R_{shunt}	20mΩ
Inductor Core Geometry	Planar EI38
Inductor Core Material	Ferroxcube 3F4
Switching Frequency	120 kHz - 750 kHz

magnetic path length. The core material parameters K, α and β are provided by the core manufacturer.

Using BCM modulation, ZVS is achieved throughout the line cycle; the switching losses are primarily turn off losses. All the switches are implemented using GaN-GIT devices from Panasonic Corporation. Thus, the turn off loss is estimated using the model developed in [23] for ZVS GaN GIT device operating in a low and high frequency bridge leg applications. It is important to note that deadtime optimization is not part of this work and the loss analysis does not include reverse conduction losses at different operating point. As illustrated in Fig. 13, the bipolar-unipolar switching technique yields a higher efficiency when compared with the standard bipolar switched BCM inverter.

V. DESIGN AND EXPERIMENTAL RESULTS

An experimental prototype of the bipolar-unipolar switched BCM inverter is constructed and shown in Fig. 14. The additional phase leg with the second inductor is populated on a second identical board and connected in parallel. The main design parameters are listed in Table I. To ensure ZVS through the entire line cycle, a fixed dead time of 100 ns and a fixed reverse ZVS current of 1.5 A is used. The inverter switching frequency varies from 120 kHz to 750 kHz, maintaining ZVS

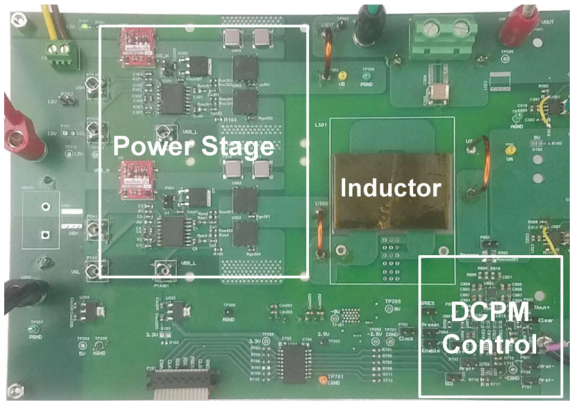

Fig. 14. Experimental prototype board.

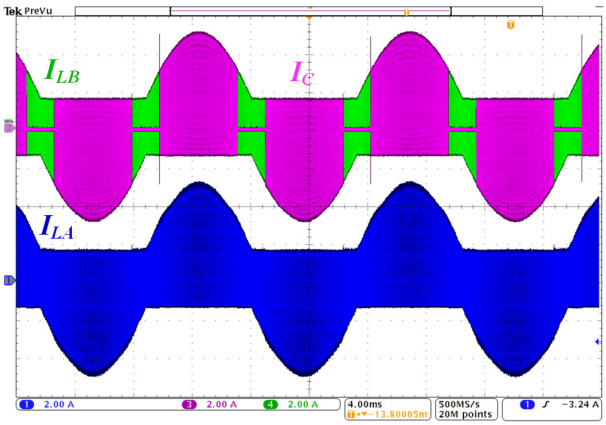

Fig. 15. Experimental phase leg A inductor current I_{LA}, phase leg B inductor current I_{LB}, and phase leg C current I_C waveform using the proposed bipolar-unipolar switched BCM inverter for $I_{out,rms}$ = 1.15 A.

at all operating points over the line cycle. The power stage has been implemented using GaN-GIT devices from Panasonic Corporation and a XILINX Spartan 6 FPGA for the digital logic and control. The inductor positive and negative current limits $I_{L,+}$ and $I_{L,-}$, are set using voltage references and regulated using a dual current programmed mode (DCPM) controller circuit outlined in [24]. Waveforms of the converter under BCM modulation with a combination of both bipolar and unipolar switching are shown in Fig. 15 for an output current RMS of 1.15 A.

To provide a comparison for the proposed switching scheme, a standard bipolar switched BCM modulation is implemented on the same prototype board. The obtained inductor current and output current waveform for both switching approaches are nearly identical and is shown in Fig. 16. At 200 W, the measured efficiency for the bipolar-unipolar switching is 93.9% and the output current THD is 1.15%. In contrast, for the fully bipolar switching, the measured efficiency at the same power level is 91.8% and the THD is 0.85%.

The proposed bipolar-unipolar switched BCM inverter

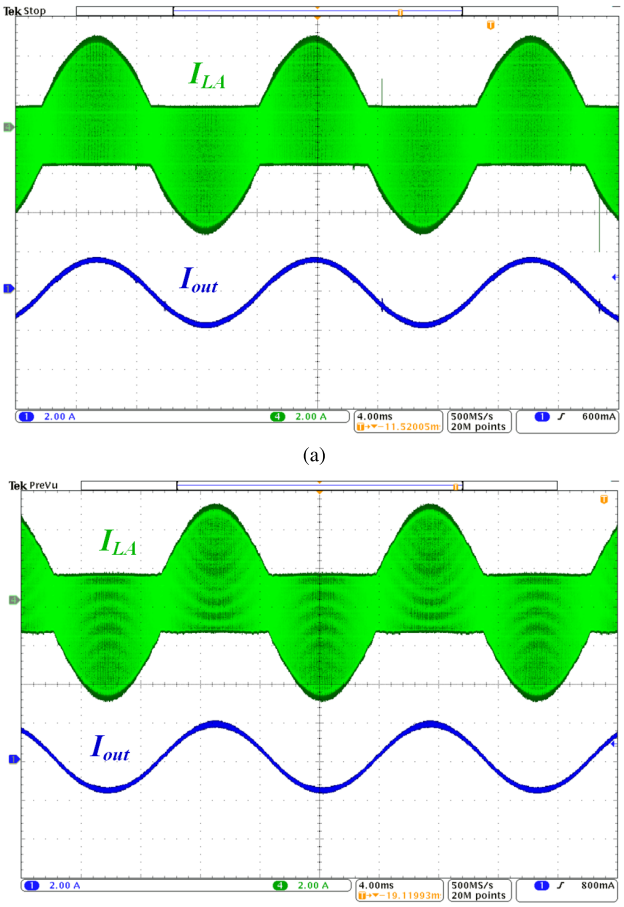

Fig. 16. Experimental phase leg A inductor current I_{LA} and output current I_{out} waveform using (a) proposed bipolar-unipolar switching and (b) standard bipolar switching for $I_{out,rms}$ = 1.15 A.

yielded a 2% improvement in efficiency and a slight increase in output current THD in comparison to the standard bipolar switched BCM inverter.

VI. Conclusions and Future Work

Both unipolar and bipolar switching techniques have been analyzed individually in the context of efficiency, output current distortion, CM noise and leakage current. Unipolar switched BCM inverter yields higher efficiency, but causes a distortion of the output current at the zero crossing. On the other hand, bipolar switched BCM inverter has the advantage of minimal leakage current, and addresses inductor current regulation and distortion issues. However, it result into a lower efficiency. A ZVS BCM control inverter combining both bipolar and unipolar switching has been proposed in this paper. This technique takes advantage of the high efficiency operation of the unipolar switching with the better inductor current regulation of the bipolar switching at the zero crossing. To mitigate the high frequency CM noise and resonance issue, a full bridge inverter with a dedicated phase leg for each switching phase has been introduced. The design and implementation of the proposed switching technique is demonstrated in an experimental GaN based full bridge inverter. The performance of the proposed switching method is compared with fully bipolar switched BCM inverter. Although the proposed switching scheme increased control complexity, and the output current THD, it yielded an improved efficiency of approximately 2% at 200 W when compared with standard bipolar switched BCM inverter.

Future work will focus on improving the overall converter efficiency, control performance, and high power operation.

Acknowledgment

This work made use of the Engineering Research Center Shared Facilities supported by the Engineering Research Center Program of the National Science Foundation and DOE under NSF Award Number EEC-1041877 and the CURENT Industry Partnership Program. This material is also based upon work supported by the National Science Foundation under Grant Number 1751878.

References

[1] K. A. Kim, Y. Liu, M. Chen, and H. Chiu, "Opening the box: Survey of high power density inverter techniques from the little box challenge," *CPSS Transactions on Power Electronics and Applications*, vol. 2, no. 2, pp. 131–139, 2017.

[2] Y. Lei, C. Barth, S. Qin, W. Liu, I. Moon, A. Stillwell, D. Chou, T. Foulkes, Z. Ye, Z. Liao, and R. C. N. Pilawa-Podgurski, "A 2 kw, single-phase, 7-level, gan inverter with an active energy buffer achieving 216 w/in3 power density and 97.6Applied Power Electronics Conference and Exposition (APEC), March 2016, pp. 1512–1519.

[3] C. Zhao, B. Trento, L. Jiang, E. A. Jones, B. Liu, Z. Zhang, D. Costinett, F. F. Wang, L. M. Tolbert, J. F. Jansen, R. Kress, and R. Langley, "Design and implementation of a gan-based, 100-khz, 102-w/in3single-phase inverter," *IEEE Journal of Emerging and Selected Topics in Power Electronics*, vol. 4, no. 3, pp. 824–840, Sep. 2016.

[4] A. Knott, T. M. Andersen, P. Kamby, J. A. Pedersen, M. P. Madsen, M. Kovacevic, and M. A. E. Andersen, "Evolution of very high frequency power supplies," *IEEE Journal of Emerging and Selected Topics in Power Electronics*, vol. 2, no. 3, pp. 386–394, Sept 2014.

[5] D. Bortis, D. Neumayr, and J. W. Kolar, "$\eta\alpha$-pareto optimization and comparative evaluation of inverter concepts considered for the google little box challenge," in *2016 IEEE 17th Workshop on Control and Modeling for Power Electronics (COMPEL)*, June 2016, pp. 1–5.

[6] D. Zhang, Q. Zhang, H. Hu, A. Grishina, J. Shen, and I. Batarseh, "High efficiency current mode control for three-phase micro-inverters," in *2012 Twenty-Seventh Annual IEEE Applied Power Electronics Conference and Exposition (APEC)*, Feb 2012, pp. 892–897.

[7] T. Isobe, K. Kato, N. Kojima, and R. Shimada, "Soft-switching single-phase grid-connecting converter using dcm operation and a turn-off snubber capacitor," *IEEE Transactions on Power Electronics*, vol. 29, no. 6, pp. 2922–2930, June 2014.

[8] A. Amirahmadi, H. Hu, A. Grishina, Q. Zhang, L. Chen, U. Somani, and I. Batarseh, "Hybrid zvs bcm current controlled three-phase microinverter," *IEEE Transactions on Power Electronics*, vol. 29, no. 4, pp. 2124–2134, April 2014.

[9] Q. Zhang, H. Hu, D. Zhang, X. Fang, Z. J. Shen, and I. Bartarseh, "A controlled-type ZVS technique without auxiliary components for the low power DC/AC inverter," *IEEE Transactions on Power Electronics*, vol. 28, no. 7, pp. 3287–3296, July 2013.

[10] J. Biela, D. Hassler, J. Minibck, and J. W. Kolar, "Optimal design of a 5kw/dm3 / 98.3rectifier," in *The 2010 International Power Electronics Conference - ECCE ASIA -*, June 2010, pp. 1709–1716.

[11] A. Amirahmadi, L. Chen, U. Somani, H. Hu, N. Kutkut, and I. Bartarseh, "High efficiency dual-mode current modulation method for low-power dc/ac inverters," *IEEE Transactions on Power Electronics*, vol. 29, no. 6, pp. 2638–2642, June 2014.

[12] B. Su, J. Zhang, and Z. Lu, "Totem-pole boost bridgeless PFC rectifier with simple zero-current detection and full-range ZVS operating at the boundary of DCM/CCM," *IEEE Transactions on Power Electronics*, vol. 26, no. 2, pp. 427–435, Feb 2011.

[13] J. Sun, X. Huang, N. N. Strain, D. J. Costinett, and L. M. Tolbert, "Inductor design and zvs control for a gan-based high efficiency crm totem-pole pfc converter," in *2019 IEEE Applied Power Electronics Conference and Exposition (APEC)*, March 2019, pp. 727–733.

[14] L. Bowtell and T. Ahfock, "Comparison between unipolar and bipolar single phase gridconnected inverters for pv applications," in *2007 Australasian Universities Power Engineering Conference*, Dec 2007, pp. 1–5.

[15] B. Ji, J. Wang, and J. Zhao, "High-efficiency single-phase transformerless pv h6 inverter with hybrid modulation method," *IEEE Transactions on Industrial Electronics*, vol. 60, no. 5, pp. 2104–2115, May 2013.

[16] B. Yang, W. Li, Y. Gu, W. Cui, and X. He, "Improved transformerless inverter with common-mode leakage current elimination for a photovoltaic grid-connected power system," *IEEE Transactions on Power Electronics*, vol. 27, no. 2, pp. 752–762, Feb 2012.

[17] W. Li, Y. Gu, H. Luo, W. Cui, X. He, and C. Xia, "Topology review and derivation methodology of single-phase transformerless photovoltaic inverters for leakage current suppression," *IEEE Transactions on Industrial Electronics*, vol. 62, no. 7, pp. 4537–4551, July 2015.

[18] D. Dong, F. Luo, D. Boroyevich, and P. Mattavelli, "Leakage current reduction in a single-phase bidirectional acdc full-bridge inverter," *IEEE Transactions on Power Electronics*, vol. 27, no. 10, pp. 4281–4291, Oct 2012.

[19] T. Wu, C. Kuo, K. Sun, and H. Hsieh, "Combined unipolar and bipolar pwm for current distortion improvement during power compensation," *IEEE Transactions on Power Electronics*, vol. 29, no. 4, pp. 1702–1709, April 2014.

[20] S. V. Araujo, P. Zacharias, and R. Mallwitz, "Highly efficient single-phase transformerless inverters for grid-connected photovoltaic systems," *IEEE Transactions on Industrial Electronics*, vol. 57, no. 9, pp. 3118–3128, Sep. 2010.

[21] J. D. Pollock and C. R. Sullivan, "Loss models for shaped foil windings on low-permeability cores," in *2008 IEEE Power Electronics Specialists Conference*, June 2008, pp. 3122–3128.

[22] ——, "Modelling foil winding configurations with low ac and dc resistance," in *2005 IEEE 36th Power Electronics Specialists Conference*, June 2005, pp. 1507–1512.

[23] D. Bortis, O. Knecht, D. Neumayr, and J. W. Kolar, "Comprehensive evaluation of gan git in low- and high-frequency bridge leg applications," in *2016 IEEE 8th International Power Electronics and Motion Control Conference (IPEMC-ECCE Asia)*, May 2016, pp. 21–30.

[24] K. Sabi and D. Costinett, "Noise mitigation and delay compensation in high frequency dual current programmed mode control," in *2018 IEEE Applied Power Electronics Conference and Exposition (APEC)*, March 2018, pp. 3095–3101.